PHYSICAL REVIEW B VOLUME 43, NUMBER 12 15 APRIL 1991-II

Transient nucleation following pulsed-laser melting of thin silicon films

S. R. Stiffler* and Michael O. Thompson
Department of Materials Science and Engineering, Cornell University, Itahaca, New York 14853

P. S. Peercy
Sandia National Laboratories, Albuquerque, New Mexico 87185-5800
(Received 26 November 1990)

Thin Si films on thermally grown SiO_2 layers were completely melted by pulsed-laser irradiation. The molten films cool very rapidly ($>10^9$ K/s) until bulk nucleation initiates solidification. The quench rate was varied by changing the thickness of the Si or the SiO_2 layers. For quenches below $\sim 10^{10}$ K/s the supercooling prior to nucleation was constant and ~ 500 K; however, for more rapid quenches, the supercooling increases significantly. This increase is attributed to embryo distributions that fall out of steady state during rapid quenches.

It has recently been shown that pulsed-laser melting of thin films allows the study of nucleation phenomena in various quench-rate and temperature regimes.[1-3] Melting thin films on nonreactive substrates by pulsed-laser radiation yields large thermal gradients in the underlying substrate which cause the molten film film to cool very rapidly ($>10^9$ K/s) until solid-phase nucleation and solidification. As a result of the very high quench rates, these experiments are sensitive to bulk nucleation rates of $\sim 10^{29}$ events/m^3 s, some 20 orders of magnitude greater than those in droplet nucleation experiments. Under these conditions, Si films on SiO_2 underlayers have been supercooled by ~ 500 K prior to uniform, bulk nucleation of the crystalline phase. Analysis of these data using steady-state homogeneous nucleation theory,[4] assuming spherical nuclei and bulk thermodynamic parameters, yields a liquid-crystal interfacial energy of 0.34 ± 0.02 J/m^2, in good agreement with Si droplet experiments.[5] Theoretical estimates indicate that, for homogeneous nucleation, embryo equilibration occurs on a nanosecond time scale.[2,4] Since cooling and embryo equilibration occur on similar time scales, effects due to embryo equilibration processes are expected to be observable in this quench-rate regime. In the following, we report the observation of transient nucleation resulting from extremely high quench rates in liquid Si.

The quench rate of a molten surface film is determined by thermal flux to the substrate and the thermal capacity of the film. For identical irradiation conditions, the thermal flux out of the molten film is determined by the thermal properties of the underlying structure. Computer simulations show that for the substrates used in these experiments (SiO_2 on Si), the heat transfer is strongly dependent on the thickness of the SiO_2 layer. Thus, the thermal flux out of the thin film can be varied by changing the thickness of the SiO_2 underlayer. Since the thermal capacity of the film is proportional to its thickness, the quench rate can be independently varied by changing the thickness of the surface Si film or the SiO_2 underlayer.

Polycrystalline Si films were deposited by chemical vapor deposition to thicknesses from 200 to 400 nm onto thermally grown layers of SiO_2 on a {100} Si substrate. The thickness of the SiO_2 layer was varied between 77 and 330 nm. The Si films were then patterned to form transient-conductance devices with aluminum contacts[6] and were completely melted with a *Q*-switched ruby laser (25–30-ns pulses at a wavelength of 694 nm). The melting and subsequent resolidification were monitored *in situ* using transient electrical conductance and transient optical reflectance.[7]

Uniform, bulk nucleation in Si leads to rapid and simultaneous decreases in both the conductance and reflectance signals as the metallic liquid transforms to the semiconducting solid.[1,2] Nucleation is followed by rapid growth into the highly cooled liquid, releasing enthalpy and reheating the film to near the melting temperature of the solid. Following recalescence, the rate of solidification is determined by the thermal properties of the underlying structure. The transition from recalescence to steady-state solidification is marked by a clear break in slope of the conductance trace. Typical conductance and reflectance data are shown in Fig. 1, with all pertinent regions labeled.

The volume fraction of solid present following recalescence (x_{rec}) can be determined from the ratio of the conductance following recalescence to the fully liquid value by assuming a specific structure of the two-phase mixture and knowledge of the relative conductivities of the two phases.[8] A microstructural model of randomly distributed crystalline inclusions in a continuous liquid matrix[9] is used and is consistent with *in situ* measurements and subsequent microstructural analysis.[1,2] This model requires a random distribution of inclusions in a continuous matrix and makes no assumptions of the specific structure of these inclusions. The requirement of a continuous matrix becomes questionable for $\chi_{rec} \gtrsim 0.52$, as spherical inclusions would then begin touching. The volume fraction of liquid consumed during recalescence can be used to determine the temperature of the liquid prior to nu-

 ©1991 The American Physical Society

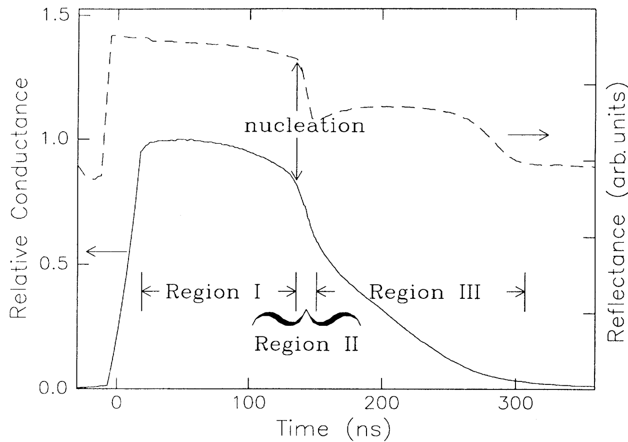

FIG. 1. Transient conductance and reflectance traces for a 300-nm Si film on a 310-nm SiO_2 underlayer irradiated with 1.07 J/cm^2. After melting, the film remains fully molten as it cools by conduction to the substrate (Region I). Nucleation of the crystalline phase initiates solidification and is indicated by the arrows. Nucleation is followed by rapid solidification (Region II) as the enthalpy released heats the film to the steady-state solidification temperature determined by the thermal properties of the substrate. Recalescence is followed by steady-state solidification (Region III). The film is fully solid at the end of Region III.

cleation (T_n) through the following heat balance:

$$t_{\mathrm{Si}}\chi_{\mathrm{rec}}\Delta H_m = t_{\mathrm{Si}}\int_{T_n}^{T_{\mathrm{SS}}} c_p(T)dT + Q_1 \ , \tag{1}$$

where t_{Si} is the thickness of the silicon film, $\Delta H_m = 4202$ J/cm^3 is the enthalpy of melting,[10] T_{SS} is the steady-state solidification temperature, $c_p(T) = 2.005 + 0.000\,29T(\mathrm{K})$ J/cm^3K is the temperature-dependent heat capacity of the liquid,[11] and Q_1 is the thermal leakage during recalescence. Equation (1) states that the total energy liberated during recalescence either heats the film or is lost by conduction to the substrate.

During steady-state solidification, the heat loss to the substrate is exactly balanced by the release of enthalpy in the solidifying film. Thus, the thermal flux out of the thin film following recalescence $\hat{q}$ may be obtained from the slope of the conductance trace immediately following recalescence. The slope of the conductance trace is a convolution of the volumetric conservation rate of liquid to solid with the specific microstructure and relative conductivities. Hence, this slope coupled with the derivative of the conductance versus composition evaluated at χ_{rec} allows determination of the volumetric conversion rate of liquid to solid immediately following recalescence. Since this volumetric conversion rate is driven by the external heat loss, it can be directly converted to a thermal flux through the enthalpy of melting in a straightforward fashion. Details of this procedure are given elsewhere.[12]

For the structure under consideration, simulations show that the heat transfer out of the surface film depends primarily on the thickness of the oxide layer and the temperature difference across it. These simulations show that the temperature at the substrate-SiO_2 interface remains nearly constant during the experiment after a few tens of nanoseconds required to heat the oxide layer. This is due to the large thermal conductivity of the relatively cool Si substrate compared to the oxide layer. The thermal flux following recalescence is an upper limit to that during recalescence since, as will be shown, T_{SS} is substantially greater than T_n. More simply put, the surface film is coolest immediately prior to nucleation, and hence the heat transfer is slowest. As rapid solidification heats the surface film, the heat transfer becomes more rapid and approaches the steady-state value as the temperature of the film approaches T_{SS}. Thus, an upper limit for the thermal leakage during recalescence can be given as

$$\hat{q}\tau_{\mathrm{rec}} \gtrsim Q_1 \ , \tag{2}$$

where τ_{rec} is the duration of the recalescence period. This thermal flux can also be used to establish an upper limit for the quench rate of the film prior to nucleation (ζ) as follows:

$$\frac{\hat{q}}{\bar{c}_p t_{\mathrm{Si}}} \gtrsim \zeta \ , \tag{3}$$

where $\bar{c}_p$ is the specific heat averaged over the temperature range of interest.

Finally, T_{SS} can be estimated from $\hat{q}$. In laser melting experiments where single-crystal Si layers are partially melted and then epitaxially regrown from the liquid, the resolidification velocity is an approximately linear function of the deviation of the liquid-solid interface from the melting temperature T_m with a slope of approximately 15 K per m/s.[13] An effective interface velocity v_{eff} can be defined as

$$v_{\mathrm{eff}} = \frac{\hat{q}}{\Delta H_m} \ , \tag{4}$$

and T_{SS} is given by

$$T_{\mathrm{SS}} = T_m - 15\frac{Ks}{m}v_{\mathrm{eff}} \ . \tag{5}$$

In the present experiments, v_{eff} varies from 1.1 to 2.4 m/s, so steady-state solidification occurs very near T_m. Values for v_{eff} agree well with the actual resolidification velocity when the surface Si films are only partially melted.

The results of these experiments are summarized in Table I. Of particular interest are the final two columns—the supercooling prior to nucleation and the quench rate—shown graphically in Fig. 2. As shown, the supercooling prior to nucleation is nearly constant and ~ 500 K for quench rates below $\sim 10^{10}$ K/s; however, it increases significantly for more rapid quenches, reaching 655 ± 80 K at $\sim 2 \times 10^{10}$ K/s. While the error bars on the data are significant, a clear trend toward increased supercoolings at higher quench rates is present. Uncertainty in the nucleation temperature of ~ 40 K at relatively low quench rates is due to the slightly different values of χ_{rec} obtained in multiple experiments. This un-

TABLE I. Compiled data for Si/SiO_2 melt-through experiments.

Group	Thicknesses (nm)	No. of samples	χ_{rec}	τ_{rec} (ns)	$\hat{q}$ (J/cm^{2}s)	Quench rate (K/s)	ΔT (K)
A	310/250	11	0.31±0.02	12±2	4.6×10^5	6.3×10^9	485±40
B	400/330	17	0.31±0.02	15±3	4.5×10^5	4.7×10^9	490±40
C	280/330	17	0.34±0.02	12±2	5.5×10^5	8.2×10^9	520±40
D	200/330	15	0.38±0.03	12±2	6.1×10^5	1.3×10^{10}	540±60
E	300/310	7	0.31±0.02	12±2	5.1×10^5	7.1×10^9	480±40
F	300/220	8	0.34±0.01	12±2	7.1×10^5	9.8×10^9	510±30
G	300/150	5	0.41±0.03	14±3	1.0×10^6	1.4×10^{10}	570±70
H	300/77	7	0.44±0.03	14±3	1.1×10^6	1.5×10^{10}	605±80
I	200/310	12	0.46±0.01	12±2	8.2×10^5	1.7×10^{10}	605±60
J	200/220	5	0.52±0.02	15±3	1.0×10^6	2.2×10^{10}	655±80
K	200/150	7			$\sim1.5\times10^6$	$\sim3.1\times10^{10}$	?
L	200/77	5			$\sim1.7\times10^6$	$\sim3.5\times10^{10}$	?

certainty increases at higher quench rates due to difficulties in evaluating the thermal leakage, as will be discussed. For this reason, analysis of the most rapid quenches (groups *K* and *L*) was not possible using the techniques outlined here, and quench rates were estimated by scaling the thermal fluxes from similar samples with thicker Si layers. The supercooling values are considered conservative, since an upper limit for the thermal leakage was used in evaluation of Eq. (1).

Increased supercoolings at higher quench rates are consistent with a nucleation process limited by embryo equilibration processes. The data in Fig. 2 suggest that, under these experimental conditions, embryo distributions are able to remain in steady-state only for quench rates slower than $\sim10^{10}$ K/s. For more rapid quenches, the embryos cannot grow at a sufficient rate to maintain a steady-state distribution. This results in fewer embryos of critical size at a supercooling of ~500 K, hence cooling continues until a sufficient number of critical nuclei are encountered at some lower temperature. The limiting case to this behavior is a quench so rapid that the embryo distribution remains static after melting. Whether elemental glasses can be formed under these conditions, or whether nucleation of a thermodynamically stable or metastable phase occurs, depends critically on the distributions of very small embryos ($\approx$ten atoms) in a superheated liquid—a case where spherical clusters and bulk thermodynamic parameters are not expected to accurately describe these distributions.

While more rapid quenches are easily attainable in these experiments, analysis using the techniques outlined above is hampered by the very large volume fraction of the liquid which is consumed during recalescence. This creates a continuous solid layer prior to steady-state solidification, causing a drastic decrease in the conductance level. An example of such data is given in Fig. 3. These data lack the well-defined transition from recalescence to steady-state solidification apparent in Fig. 1, making accurate determination of χ_{rec} and τ_{rec} difficult and leading to larger uncertainties in Q_l. These

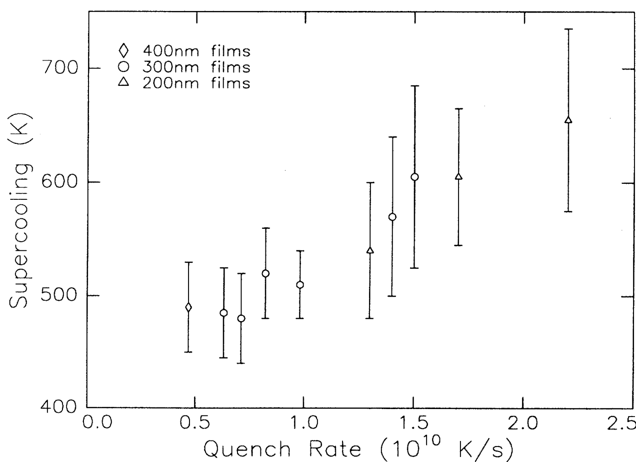

FIG. 2. Supercooling prior to nucleation as a function of quench rate. Note that the quench rate presented here is an upper limit and the supercooling is a lower limit.

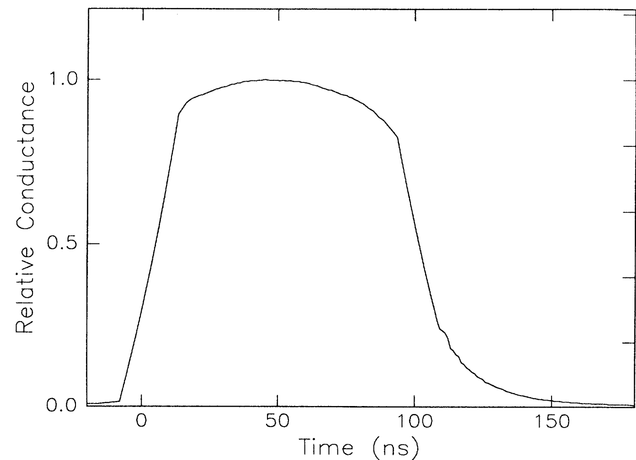

FIG. 3. Transient conductance trace of a 200-nm Si film on a 150-nm SiO_2 layer (sample group *K*). Note the dramatic decrease in conductance following nucleation and the absence of a break in slope associated with the transition to steady-state solidification apparent in Fig. 1.

difficulties are responsible for larger uncertainties in the supercooling at higher quench rates, and ultimately limit the experimental techniques outlined here.

While temperature determination using the techniques outlined previously is not possible for the most rapid quenches examined, useful information can be obtained from microstructural examination. Previous examinations[1,2] have shown microstructures consisting of randomly oriented grains of size comparable to the film thickness. This was also the case in these experiments except for the most rapidly quenched samples (groups K and L). Like previous studies, no evidence of preferential nucleation at either the free surface or at the Si/SiO_2 interface was observed; however, substantial volume fractions of extremely fine-grained (5–10 nm) material were present in addition to the fairly large grains. Figures 4 and 5 show planar and cross-sectional transmission electron micrographs from sample group I, showing a microstructure typical of the more slowly quenched samples; and from sample group L, showing a distinctly different one. Note the regions of very fine-grained material interspersed among the relatively coarse grains in Figs. 4(b) and 5(b). This fine-grained material is the distinctive signature of explosive crystallization of the metastable amorphous phase.[14]

It is believed that these microstructures evolved through substantially different resolidification scenarios, consistent with nucleation at different temperatures. Specifically, it is believed that the very fine-grained material was originally amorphous and was subsequently transformed to crystalline material via explosive crystallization, as has previously been observed in similar experiments with germanium.[3] Whether the amorphous phase nucleated directly from the liquid or at a highly undercooled liquid-crystal interface during the initial stages of solidification cannot be determined unambiguously from the microstructure; however, extensive analysis by transmission electron microscopy has revealed separate sites where it appears that bulk nucleation of the amorphous and crystalline phases has occurred. Competitive

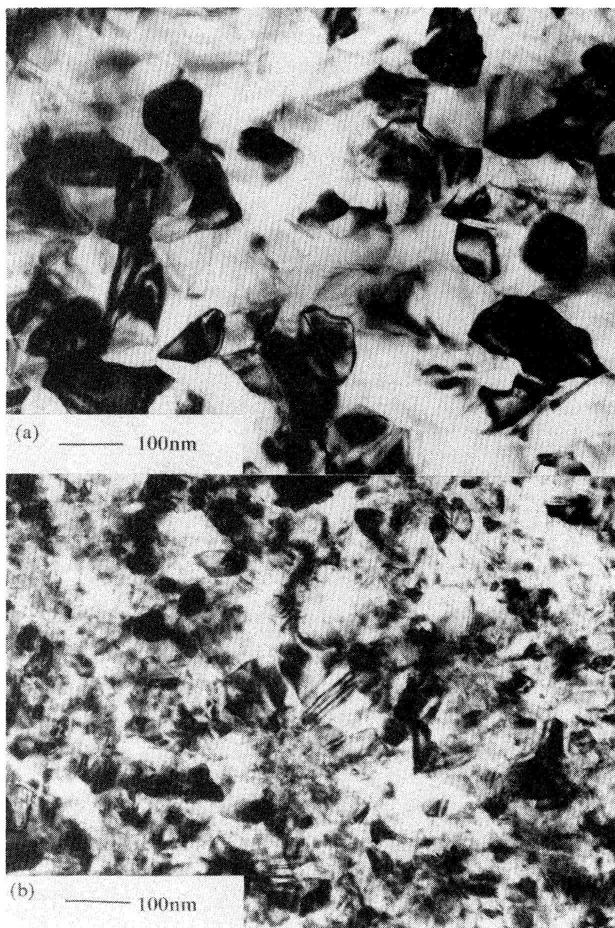

FIG. 4. Bright-field, planar transmission electron micrographs from (a) sample group I which was cooled at $\sim 1.7\times10^{10}$ K/s and (b) sample group L which was cooled at $\sim 3.5\times10^{10}$ K/s. Note the uniform grain size in (a) compared with (b) and the distinct regions of very fine-grained material in (b).

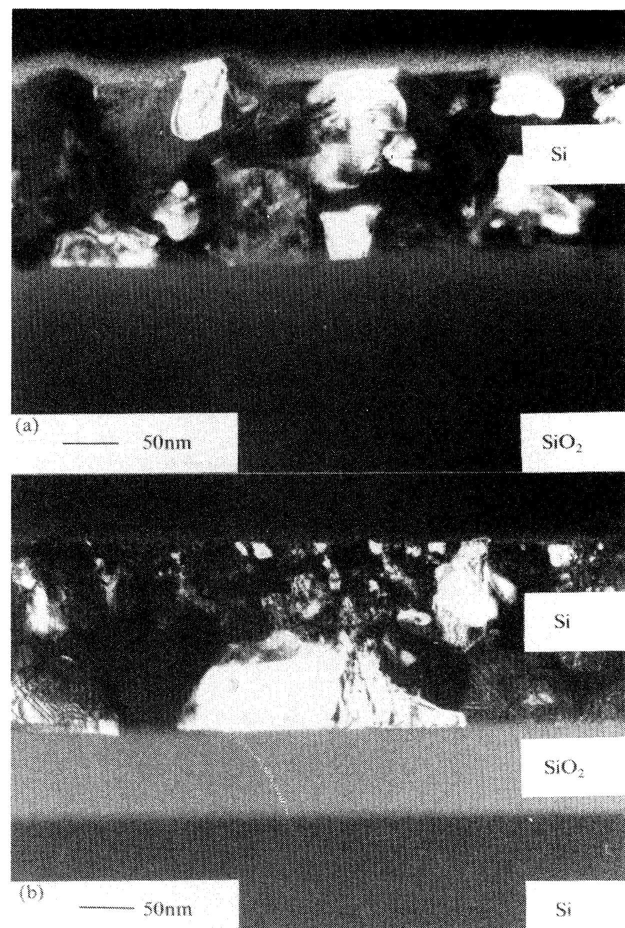

FIG. 5. Dark field, cross-sectional transmission electron micrographs from (a) sample group I and (b) sample group L. The cooling rates were $\sim 1.7\times10^{10}$ K/s and $\sim 3.5\times10^{10}$ K/s, respectively. Note no evidence of preferential nucleation at either the free surface or the Si/SiO_2 interface in either sample and the very fine-grained regions in (b).

nucleation between these phases is not unexpected in this temperature range, based upon recent estimates of the amorphous-liquid interfacial energy in silicon.[15] In fact, Sameshima and co-workers[16,17] recently reported complete amorphization of very thin silicon films (20–40 nm) on quartz substrates following melting with 30-ns excimer laser pulses. It is estimated that these films were quenched at rates slightly greater than the most rapid cases in the present work. These films were determined to be the semiconducting, amorphous phase, as opposed to a configurationally frozen liquid or glassy structure, which would be metallic.[18]

While the various experiments examining the solidification of silicon at different rates[1,5,15,17] have yielded different results, together they generate a consistent scenario regarding the nucleation of a solid phase (crystalline or amorphous) in the highly cooled liquid. If care is taken to eliminate heterogeneous nucleation, at slow[5] to moderate[1] cooling rates, solidification is initiated by bulk solidification of the crystalline phase. As a result of the different cooling rates and volumes of liquid, the supercooling prior to nucleation in these experiments was 285 K (Ref. 5) and 500 K (Ref. 1); however, analysis using steady-state homogeneous nucleation theory yields nearly identical values for the liquid-crystal interfacial energy. As the quench rate is further increased to near 10^{10} K/s, the supercooling prior to nucleation increases in a manner inconsistent with steady-state nucleation. Associated with this increased supercooling is a distinctly different microstructure, indicating that the amorphous phase was present at some time during the solidification process. Based on the results of Evans *et al.*,[15] it is believed that this microstructure results from competitive nucleation between the crystalline and amorphous phases due to the deeper supercoolings associated with transient nucleation. As the quench rate is further increased,[16,17] or as the nucleating volume is decreased,[15] nucleation of the amorphous phase initiates solidification. Whether further increases in the quench rate will produce a configurationally frozed liquid remains to be seen.

In conclusion, experiments examining the quench-rate dependence of solid phase nucleation in liquid Si show that the supercooling prior to nucleation remains nearly constant below a quench rate of $\sim 10^{10}$ K/s. For more rapid quenches, the supercooling prior to nucleation increases significantly, providing the first experimental information on the rate of embryo equilibrium processes in elemental liquids. For the most rapid quench rates, analysis shows a substantially different microstructure, consistent with nucleation in a cooler liquid.

We gratefully acknowledge the laboratory assistance of R. Blake at Sandia. Work at Cornell is supported by NSF-PYIA (J. Hurt) and samples were fabricated at the National Nanofabrication Facility (NSF) at Cornell. Work at Sandia is supported by Grant No. DE-AC04-76DP00789.

*Present address: IBM Thomas J. Watson Research Center, Yorktown Heights, NY 10598-0218.

[1]S. R. Stiffler, M. O. Thompson, and P. S. Peercy, Phys. Rev. Lett. **60**, 2519 (1988).

[2]S. R. Stiffler, M. O. Thompson, and P. S. Peercy, in *Fundamentals of Beam-Solid Interactions and Transient Thermal Processing,* edited by M. J. Aziz, L. E. Rehn, and B. Stritzer, MRS Symposia Proceedings No. 100 (Materials Research Society, Pittsburgh, 1988), p. 505.

[3]S. R. Stiffler, M. O. Thompson, and P. S. Peercy, Appl. Phys. Lett. **56**, 1025 (1990).

[4]J. W. Christian, *The Theory of Transformations in Metals and Alloys* (Pergamon, Oxford, 1965), pp. 377.

[5]G. Devaud and D. Turnbull, Appl. Phys. Lett. **46**, 844 (1985).

[6]G. J. Galvin, M. O. Thompson, J. W. Mayer, R. B. Hammons, N. Paulter, and P. S. Peercy, Phys. Rev. Lett. **48**, 33 (1982).

[7]D. H. Auston, C. M. Surko, T. N. C. Venkatesan, R. E. Slusher, and J. A. Golovchenko, Appl. Phys. Lett. **33**, 437 (1978).

[8]*Electrical Conductivity in Ceramics and Glass, Part B,* edited by N. M. Tallman (Decker, New York, 1974), p. 624.

[9]D. A. G. Bruggeman, Ann. Phys. (Leipzig) **24**, 636 (1935).

[10]*Properties of Silicon,* EMIS Datareview Series No. 4 (Inspec, London, 1988), p. 57.

[11]Y. S. Touloukian and E. H. Buyco, *Specific Heat, Metallic Elements and Alloys,* Vol. 4 of *Thermophysical Properties of Matter* (IFI/ Plenum, New York, 1970).

[12]S. R. Stiffler, Ph.D. thesis, Cornell University, 1988.

[13]M. O. Thompson P. H. Bucksbaum, and J. Bokor, in *Energy-Beam Solid Interactions and Transient Thermal Processing,* edited by D. K. Biegelsen, G. A. Ruzgonyi, and C. V. Shank, MRS Symposia Proceedings No. 35 (Materials Research Society, Pittsburgh, 1985), p. 181.

[14]See, for example, D. H. Lowndes *et al.*, J. Mater. Res. **2**, 648 (1987).

[15]P. V. Evans, G. Devaud, T. F. Kelly, and Y-W. Kim, Acta Metall. Mater. **38**, 719 (1990).

[16]T. Sameshima, M. Hara, and S. Usui, Jpn. J. Appl. Phys. **29**, L548 (1990).

[17]T. Sameshima, M. Hara, N. Sano, and S. Usui, Jpn. J. Appl. Phys. **29**, L1363 (1990).

[18]V. M. Glazov, S. N. Chizhevskaya, and N. N. Glagoleva, *Liquid Semiconductors* (Plenum, New York, 1969).

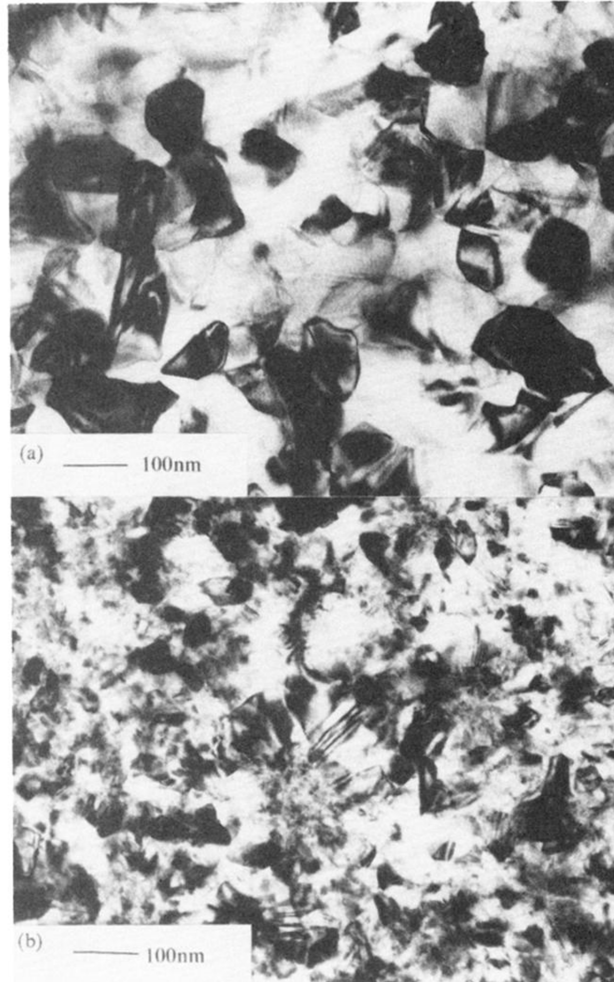

FIG. 4. Bright-field, planar transmission electron micrographs from (a) sample group *I* which was cooled at $\sim 1.7\times 10^{10}$ K/s and (b) sample group *L* which was cooled at $\sim 3.5\times 10^{10}$ K/s. Note the uniform grain size in (a) compared with (b) and the distinct regions of very fine-grained material in (b).

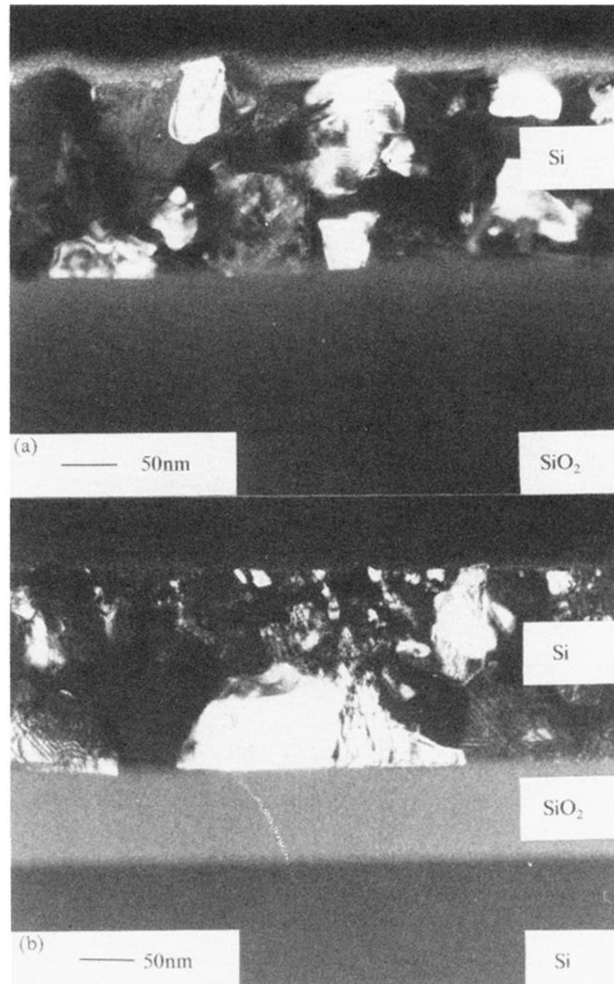

FIG. 5. Dark field, cross-sectional transmission electron micrographs from (a) sample group *I* and (b) sample group *L*. The cooling rates were $\sim 1.7\times 10^{10}$ K/s and $\sim 3.5\times 10^{10}$ K/s, respectively. Note no evidence of preferential nucleation at either the free surface or the Si/SiO_2 interface in either sample and the very fine-grained regions in (b).